Satellite chartography of atmospheric methane from SCIAMACHY on board ENVISAT: Analysis of the years 2003 and 2004

C. Frankenberg,[1] J. F. Meirink,[2] P. Bergamaschi,[3] A. P. H. Goede,[2] M. Heimann,[4] S. Körner,[4] U. Platt,[1] M. van Weele,[2] and T. Wagner[1]

Received 18 May 2005; revised 1 December 2005; accepted 23 January 2006; published 8 April 2006.

[1] The UV/Vis/near infrared spectrometer SCIAMACHY on board the European ENVISAT satellite enables total column retrieval of atmospheric methane with high sensitivity to the lower troposphere. The vertical column density of methane is converted to column averaged mixing ratio by using carbon dioxide retrievals as proxy for the probed atmospheric column. For this purpose, we apply concurrent total column measurements of CO_2 in combination with modeled column-averaged CO_2 mixing ratios. Possible systematic errors are discussed in detail while the precision error is 1.8% on average. This paper focuses on methane retrievals from January 2003 through December 2004. The measurements with global coverage over continents are compared with model results from the chemistry–transport model TM4. In the retrievals, the north-south gradient as well as regions with enhanced methane levels can be clearly identified. The highest abundances are found in the Red Basin of China, followed by northern South America, the Gangetic plains of India and central parts of Africa. Especially the abundances in northern South America and the Red Basin are generally higher than modeled. Further, we present the seasonal variations within the investigated time period. Peak values in Asia due to rice emissions are observed from August through October. We expand earlier investigations that suggest underestimated emissions in the tropics. It is shown that these underestimations show a seasonal behavior that peaks from August through December. The global measurements may be used for inverse modeling and are thus an important step towards better quantification of the methane budget.

Citation: Frankenberg, C., J. F. Meirink, P. Bergamaschi, A. P. H. Goede, M. Heimann, S. Körner, U. Platt, M. van Weele, and T. Wagner (2006), Satellite chartography of atmospheric methane from SCIAMACHY on board ENVISAT: Analysis of the years 2003 and 2004, *J. Geophys. Res.*, *111*, D07303, doi:10.1029/2005JD006235.

1. Introduction

[2] Methane (CH_4) is, after carbon dioxide, the second most important anthropogenic greenhouse gas, contributing directly 0.48 W m^{-2} to the total anthropogenic radiative forcing of 2.43 W m^{-2} by well-mixed greenhouse gases [*IPCC*, 2001, and references therein]. In addition, it exhibits an indirect effect of about 0.13 W m^{-2} through formation of other greenhouse gases, most notably tropospheric ozone and stratospheric water vapor [*Lelieveld et al.*, 1998]. In contrast to these abundance based radiative forcing estimates, *Shindell et al.* [2005] calculated the overall forcing based on emissions, thereby accounting for all indirect effects. From the emissions-based viewpoint, they conclude that the impact of anthropogenic methane on radiative forcing is larger than previously estimated, namely about 0.8 W m^{-2}.

[3] Since the beginning of industrialization, methane abundances in the atmosphere have more than doubled [*Etheridge et al.*, 1998] albeit with decreasing growth rate [*Dlugokencky et al.*, 1998] during the past two decades and considerable inter-annual variations [*Dlugokencky et al.*, 2001]. Furthermore, there is evidence that natural methane emissions have a positive feedback from rising temperatures [*Worthy et al.*, 2000; *Gedney et al.*, 2004; *Shindell et al.*, 2004], leading to expectations of a further increase in methane abundances. Reduction of methane emissions could at present be a cost-effective and feasible strategy for reducing positive radiative forcing [*Hansen et al.*, 2000; *Hansen and Sato*, 2004]. Hence, better knowledge of methane distribution and emissions is indispensable for a correct assessment of its impact on climate as well as on the chemical composition of the atmosphere [*Dentener et al.*, 2005] through, e.g., a reduction of the OH radical concentrations at higher methane abundances.

[1] Institute of Environmental Physics, University of Heidelberg, Heidelberg, Germany.
[2] Section of Atmospheric Composition, Royal Netherlands Meteorological Institute, De Bilt, Netherlands.
[3] European Commission Joint Research Centre, Ispra, Italy.
[4] Max Planck Institute for Biogeochemistry (MPI-BGC), Jena, Germany.

0148-0227/06/2005JD006235

Also the Kyoto protocol calls for an independent global quantification and monitoring of emissions [*IPCC*, 2000; *Bergamaschi et al.*, 2004]. According to current emission inventories, approximately 70% of global methane emissions are anthropogenic [*Lelieveld et al.*, 1998]. The largest contributors are fossil fuel production, ruminants, waste handling and rice cultivation [*Olivier and Berdowski*, 2001]. Wetlands constitute the most important natural source.

[4] Although the global annual source strength of methane (550 ± 50 Tg yr^{-1}) is comparatively well constrained, considerable uncertainties still exist in regard to the partitioning amongst sources and their spatial and temporal distribution. "Bottom-up" approaches use local flux measurements and statistical data for upscaling to global totals. This upscaling, however, may inherit large uncertainties, especially for sources with large spatial or temporal variability (e.g., CH_4 from wetlands). In contrast, "top-down" approaches use atmospheric measurements and inverse atmospheric models in order to derive estimates of sources (and sinks) [*Hein et al.*, 1997; *Houweling et al.*, 1999; *Bergamaschi et al.*, 2000; *Fletcher et al.*, 2004b; *Dentener et al.*, 2003; *Chen*, 2003; *Butler et al*,. 2004; *Fletcher et al.*, 2004a; *Bergamaschi et al.*, 2005]. A major limitation of present top-down estimates is the limited number of atmospheric observation sites. Hence, additional a priori information from bottom-up estimates is usually required in order to overcome the underdetermination of the inverse problem. As a consequence, large uncertainties still exist, especially for regions ill-sampled by the current atmospheric network, e.g., large parts of the tropics (see, for instance, the Climate Monitoring and Diagnostics Laboratory (CMDL) of the U.S. National Oceanic and Atmospheric Administration (NOAA): http://www.cmdl.noaa.gov/).

[5] Satellites offer the unique possibility of sensing methane globally, retrieving methane abundances in remote areas where ground based measurements might be complicated or even impossible due to infrastructural or political obstacles. The atmospheric lifetime of methane, mainly determined by oxidation due to OH radicals, is relatively long, namely, about 8 years [*IPCC*, 2001; *Lelieveld et al.*, 1998]. Consequently, methane is well mixed and its variations in time and space are rather small, demanding unprecedented precision (1–2%) for space based total column retrievals that can be employed in top-down inversions. Methane columns have been measured from space by the IMG instrument on board ADEOS [*Clerbaux et al.*, 2003] and, more recently, by the SCIAMACHY instrument on board ENVISAT [*Buchwitz et al.*, 2005a; *Frankenberg et al.*, 2005a; *Buchwitz et al.*, 2005b]. The IMG measurements were made by mid-infrared emission spectroscopy, being sensitive to methane in the free troposphere but suffering a substantially reduced sensitivity near the Earth's surface. SCIAMACHY retrievals are based on absorption spectra of solar radiation in the near-infrared. The recorded photons have traversed the entire atmospheric column twice, thereby exhibiting high sensitivity, including toward the surface. In the future, both measurement types could be combined synergistically.

[6] *Frankenberg et al.* [2005a] presented methane column retrievals from SCIAMACHY for the period August–November 2003, reporting a good overall agreement of these retrievals with model simulations. However, substantial differences were found over large parts of the continental tropics, which were attributed to an underestimation of tropical methane emissions in the model.

[7] In this work, we extend the analysis in *Frankenberg et al.* [2005a] by presenting methane retrievals for the entire years 2003 and 2004. Possible systematic errors and retrieval precision are discussed in detail. Further, considerable improvements in the retrieval and in computing a modeled column averaged mixing ratio that is directly comparable to SCIAMACHY retrievals have been elaborated.

2. SCIAMACHY Instrument

[8] SCIAMACHY (SCanning Imaging Absorption spectroMeter for Atmospheric CHartographY) [*Bovensmann et al.*, 1999] on board the European Space Agency's environmental research satellite ENVISAT consists of 8 individual grating spectrometer channels (1 through 8) measuring in the ultraviolet, visible and near infrared wavelength regions (240 nm–2380 nm) of the solar spectrum. The satellite operates in a near polar, sun-synchronous orbit at an altitude of 800 km with a local equator crossing time of approximately 10:00 am. The instrument alternates between limb and nadir modes of measurement. In the latter mode, a swath of 960 km gives full global coverage every six days (14 orbits per day). The typical ground pixel size of SCIAMACHY is 30 km (along-track, i.e., approximately north-south) times 60 to 120 km (across-track, i.e., approx. east-west). SCIAMACHY is an advanced successor of GOME (Global Ozone Monitoring Experiment) on board ERS-2, the smaller footprint being one of its major improvements. Both GOME and SCIAMACHY are equipped with UV/Vis spectrometers, enabling global detection of NO_2, BrO, OClO, H_2O, SO_2, O_3, CH_2O, O_2 and O_4 as well as providing information on clouds and aerosols [*Burrows et al.*, 1999; *Wagner et al.*, 2002].

[9] In addition to GOME, SCIAMACHY features three near infrared spectrometers (ch. 6: 1000–1750 nm, ch. 7: 1940–2040 nm, and ch. 8: 2265–2380 nm) that enable global measurements of total columns of CH_4, CO_2, N_2O and CO by means of differential optical absorption spectroscopy (DOAS) *Platt* [1994]. First results from these near infrared channels are now available from two other groups [*Buchwitz et al.*, 2004, 2005a; *Gloudemans et al.*, 2004, 2005; *Buchwitz et al.*, 2005b], using different retrieval algorithms to retrieve methane column densities from channel 8 of SCIAMACHY. Following *Frankenberg et al.* [2005a], we only used spectra from channel 6 to avoid problems due to an ice layer on the detectors of channels 7 and 8 [*Gloudemans et al.*, 2005]. In addition, channel 6 exhibits a better signal-to-noise ratio and spatial resolution (60×30 km compared to 120×30 km in channel 8) than the other near infrared channels. The only major drawback is the lower spectral resolution (FWHM approx. 1.35 nm) compared to channels 7 and 8 (FWHM approx. 0.24 nm).

[10] Figure 1 illustrates the SCIAMACHY measurement geometry in the nadir mode. Line of sight zenith angles

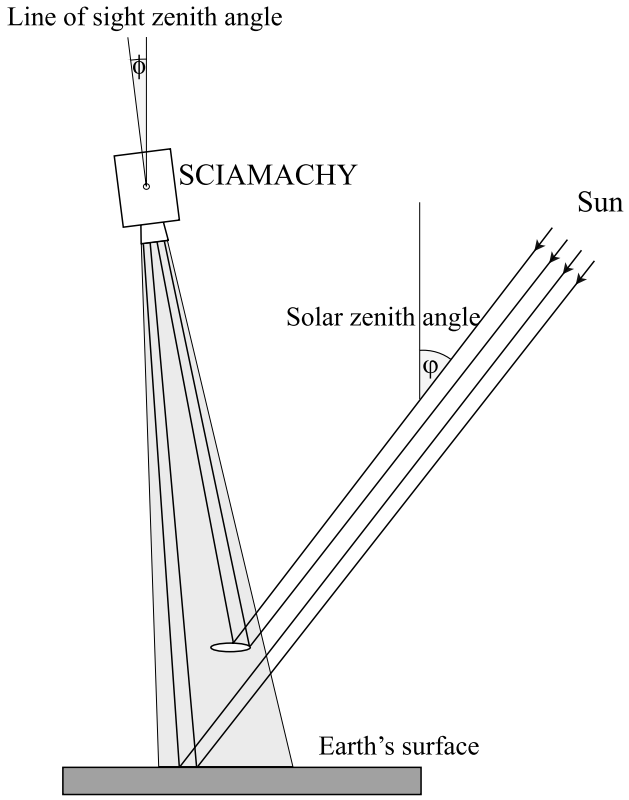

Figure 1. Schematical representation of the SCIAMACHY nadir measurement geometry. Line of sight zenith angle and solar zenith angle are abbreviated LZA and SZA, respectively.

(LZA) are off-nadir by up to 30°. In addition to these earthshine radiance measurements, direct solar irradiance measurements are performed each day.

3. Retrieval Methods

3.1. Retrieval of Vertical Column Densities

[11] We applied the iterative maximum a posteriori (IMAP) DOAS algorithm [*Frankenberg et al.*, 2005b] to retrieve vertical column densities (VCD or simply *V*, concentration integrated vertically from the surface to the top of atmosphere) of CH_4 and CO_2. A simplified radiative transfer scheme that ignores scattering is used to model a spectra that SCIAMACHY would measure given the a priori abundances of all absorbers. In our case we model optical densities, i.e., the negative logarithm of the ratio of the nadir radiance and the solar irradiance spectra. The algorithm basically performs a non-linear constrained least squares fit (based on the Optimal Estimation approach introduced by *Rodgers* [1976]), directly iterating a low order polynomial and the vertical column densities of the absorbers of interest until the modeled total optical densities fit the measurement.

[12] The algorithm and an extensive sensitivity analysis are described in detail in *Frankenberg et al.* [2005b]. A retrieval simulation was performed to study various effects with potential impact on the retrieval, for instance pressure and temperature variations in the atmosphere. These errors were shown to be mostly below 1%.

[13] The algorithm has been successfully applied to retrieve carbon monoxide [*Frankenberg et al.*, 2005c] and methane [*Frankenberg et al.*, 2005a]. In contrast to previous methane retrievals [*Frankenberg et al.*, 2005a], we use the latest edition of HITRAN (high-resolution transmission molecular absorption database, *Rothman et al.* [2005]) for the calculation of reference spectra. It comprises substantial updates especially for CO_2 lines residing in the fitting window applied in this study.

[14] Further fit parameters employed for the retrieval of the data set presented in this study are summarized in Table 1. Although we perform a total column retrieval, the vertical column densities of CH_4 and CO_2 are divided into three separate layers, where the upper two layers (from 3–12 km and 12–120 km) are tightly constrained via the a priori covariance matrix (see *Rodgers* [2000] for details). Only the constraints for the lowermost layer are noncommittal. Since the information content of the measurements is too low to retrieve different height layers independently, tight constraints for all but one layer are needed to avoid numerical instabilities.

[15] The retrieved total column, i.e., the sum of the vertical columns of all height layers, is still sensitive to variations in higher atmospheric layers but treats them as if they occurred in the lowest layer. This has important implications for the sensitivity of the retrieval with respect to concentration changes in different height layers. In our application, the averaging kernel is defined as the sensitivity of the total column retrieval to concentration perturbations with respect to the a priori at different height layers. Given the true changes in each height layer, the vertical column as retrieved by SCIAMACHY can be approximated by:

$$\hat{V} = V_a + \sum_i A^i \cdot \left(V^i - V_a^i\right), \tag{1}$$

where

$\hat{V}$ = retrieved total VCD
V_a = a priori total VCD
V^i = true VCD of height layer i
V_a^i = a priori VCD of height layer i
A^i = averaging kernel of height layer i.

[16] For weak absorbers, radiative transfer alone determines the averaging kernels; Thus, they should be equal at all heights if scattering is neglected. For strong absorbers such as CH_4 and CO_2, the sensitivity also depends on the shape of the individual absorption lines and thereby, due to pressure broadening, also on height [*Frankenberg et al.*, 2005b]. This implies that the averaging kernels depend on the choice of the state vector (vector containing the quantities to be retrieved, see *Rodgers* [2000] and *Frankenberg et al.* [2005b]).

[17] Figure 2 shows the averaging kernels for our CH_4 and CO_2 retrievals. Since the a priori covariance is noncommittal only for the lowest atmospheric layer, averaging kernels are close to unity in this layer. Thus, perturbations in this height layer are reproduced accurately and, most

Table 1. Fit Parameters as Used for the CH_4 and CO_2 Retrieval

Fit Parameter	Height Layer, km	a Priori	a Priori σ[a]
		CH_4 Fit[b]	
CH_4 (I)	0–3	$1.127 \cdot 10^{19}$ [molec/cm^2]	$1.127 \cdot 10^{19}$ [molec/cm^2]
CH_4 (II)	3–12	$1.83 \cdot 10^{19}$ [molec/cm^2]	$1.83 \cdot 10^{15}$ [molec/cm^2]
CH_4 (III)	12–120	$5.98 \cdot 10^{18}$ [molec/cm^2]	$5.98 \cdot 10^{14}$ [molec/cm^2]
CH_4 climatology[c]	0–120	0 [–]	5 [–]
H_2O	0–120	$4.773 \cdot 10^{22}$ [molec/cm^2]	$4.773 \cdot 10^{22}$ [molec/cm^2]
H_2O climatology[c]	0–120	0 [–]	5 [–]
CO_2	0–120	$7.98 \cdot 10^{21}$ [molec/cm^2]	$7.98 \cdot 10^{21}$ [molec/cm^2]
CO_2 climatology[c]	0–120	0 [–]	5 [–]
		CO_2 Fit[d]	
CO_2 (I)	0–3	$2.453 \cdot 10^{21}$ [molec/cm^2]	$2.453 \cdot 10^{21}$ [molec/cm^2]
CO_2 (II)	3–12	$3.995 \cdot 10^{21}$ [molec/cm^2]	$3.995 \cdot 10^{17}$ [molec/cm^2]
CO_2 (III)	12–120	$1.534 \cdot 10^{21}$ [molec/cm^2]	$1.534 \cdot 10^{17}$ [molec/cm^2]
CO_2 climatology[c]	0–120	0 [–]	5 [–]
H_2O	0–120	$4.773 \cdot 10^{22}$ [molec/cm^2]	$4.773 \cdot 10^{22}$ [molec/cm^2]
H_2O climatology[c]	0–120	0 [–]	5 [–]

[a] σ as given in the a priori covariance matrix, assuming zero off-diagonal elements [*Rodgers*, 2000; *Frankenberg et al.*, 2005b].
[b] Fit window: 1630.5–1669.9 nm; 2 iterations; Slit function: Gaussian, 1.35 nm FWHM; degree of polynomial: 2.
[c] As climatological fit parameter the difference between the U.S. standard atmosphere and a midlatitude winter atmosphere was taken. For details concerning the implementation, see *Frankenberg et al.* [2005b].
[d] Fit window: 1562.6–1584.6 nm; 2 iterations; Slit function: Gaussian, 1.35 nm FWHM; degree of polynomial: 2.

importantly, with equal sensitivity to both species. Deviations from the a priori in higher atmospheric layers are still retrieved, albeit with less sensitivity.

3.2. Converting Vertical Column Densities to Column Averaged Mixing Ratios

[18] If vertical column densities are to be converted to column averaged mixing ratios, we need to know the probed total atmospheric column, which, in turn, depends on pressure and light path distribution. One of the main advantages of the near infrared spectral regions is that Rayleigh scattering as well as thermal emissions can be safely ignored. In the absence of clouds and aerosols, we can thus exactly derive the path of the photons that constitute the measurement by simple geometric considerations of the measurement geometry, i.e., considering the line of sight zenith angle (LZA) and the solar zenith angle (SZA) (see Figure 1). In this simple case, we could directly convert vertical column densities to column averaged mixing ratios of CH_4 and CO_2 by scaling with the probed vertical column of all atmospheric constituents (strictly speaking without water vapor), a quantity that can be derived from surface pressure.

[19] Aerosols and clouds (as apparent in Figure 1) in the field of view complicate the retrieval [*Buchwitz et al.*, 2000;

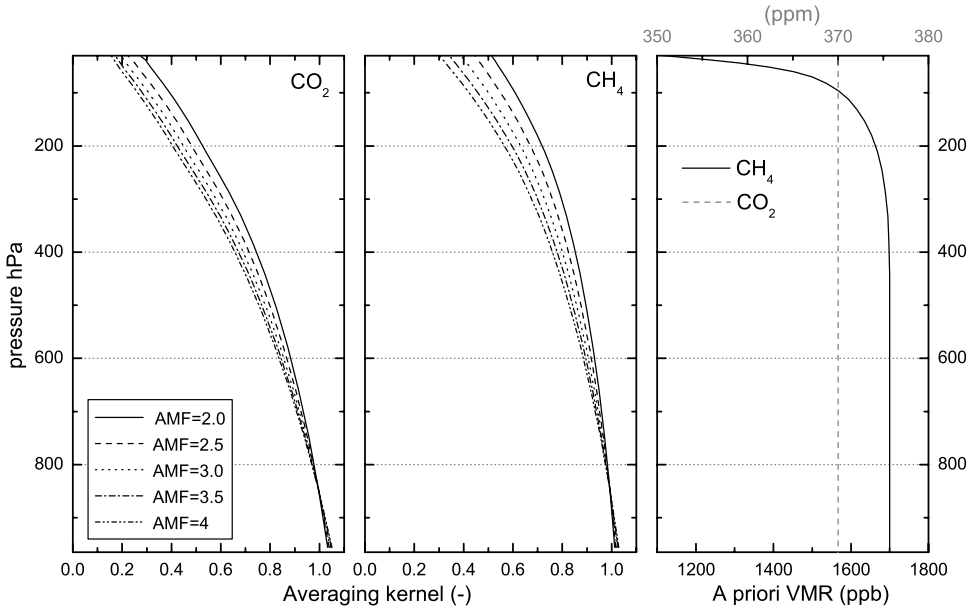

Figure 2. Averaging kernels of the IMAP DOAS retrieval of CH_4 and CO_2 for different air mass factors ($\approx$1/cos(LZA) + 1/cos(SZA)). The right panel shows the corresponding a priori profiles for which the averaging kernels have been computed (profiles from U.S. standard atmosphere provided by *Kneizys et al.* [1996]).

Buchwitz and Burrows, 2003; *O'Brien and Rayner*, 2002; *Rayner et al.*, 2002] since they substantially alter the light path and thereby the probed total column. This renders a simple scaling by surface pressure insufficient. The deviations induced by these changes in the light path are generally not large in the near infrared but the precision requirements for a meaningful retrieval of CH_4 are so strict (1–2%) that these effects have to be considered. In typical conditions, the effect of aerosols is below 2% if the surface albedo exceeds 5% [*Buchwitz and Burrows*, 2003; *Houweling et al.*, 2005]. In extreme cases, as in dust storms in the Sahara, which exhibit high optical densities even in the near infrared, the errors in the retrieved vertical columns are up to 10% and strongly depend on surface albedo [*Houweling et al.*, 2005]. Partial cloud cover further complicates the retrieval since clouds shield the atmospheric layers underneath. Since SCIAMACHY has large footprints, most pixels are partially covered by clouds, and the majority of the measurements would be rejected if strict constraints on cloud coverage were imposed.

[20] In order deal with aerosols and partial cloud cover, we have to apply a proxy for the total column of the probed atmosphere. This total vertical column of dry air (V_{air}) depends on both pressure and light path distribution. Using proxy X, V_{air} reads

$$V_{\mathrm{air}} = \frac{V(X)}{\overline{VMR}(X)}\,, \tag{2}$$

where $\overline{VMR}(X)$ denotes the column averaged mixing ratio and $V(X)$ the vertical column density of species X. Usually, spectroscopic O_2 or O_4 measurements are used as proxy [*Pfeilsticker et al.*, 1998; *Wagner et al.*, 2003] as their averaged mixing ratios are precisely known and exhibit negligible variations. However, these species absorb in very different wavelength regions (e.g., O_2: 760 nm) and are thus not directly representative for the light path distribution in the near infrared. In contrast, CO_2 is retrieved in a spectrally neighboring fitting window ensuring very similar light path distributions. In addition to the prerequisite of identical light paths, the sensitivity of the measurement to the species of interest and its proxy for the total air column has to be very similar at height levels where the largest deviations from the expected light path occur. The choice of the state vector as described above ensures nearly equal averaging kernels in the lowermost atmospheric layer. In terms of radiative transfer properties, CO_2 is thus an ideal proxy. A complication is that CO_2 exhibits variations in the column averaged mixing ratio, albeit generally below 3% [*Olsen and Randerson*, 2004]. In *Frankenberg et al.* [2005a], CO_2 retrievals were introduced as proxy for the probed column assuming a globally constant mixing ratio. Here we greatly improve this approach by considering modeled column averaged mixing ratios of carbon dioxide (see section 4.2) to diminish the systematic errors induced by variations in CO_2. The column averaged mixing ratio of methane is thus obtained by

$$\overline{VMR}(\mathrm{CH_4}) = \frac{V_{\mathrm{meas}}(\mathrm{CH_4})}{V_{\mathrm{meas}}(\mathrm{CO_2})} \cdot \overline{VMR}(\mathrm{CO_2})\,, \tag{3}$$

where $\overline{VMR}(CO_2)$ is the modeled column averaged mixing ratio of CO_2. Although the CO_2 model might not exactly represent the true value, the strongest variations, i.e., the seasonal cycle, are well reproduced.

[21] The measurements exhibit a small positive bias compared to the model simulations. To facilitate the comparison, we scale $\overline{VMR}(CH_4)$ by a constant factor (0.982). In comparison to *Frankenberg et al.* [2005a], this factor changed due to updates in applied CO_2 line parameters.

3.3. Error Analysis

[22] The derived column averaged mixing ratio is affected by statistical errors in the retrieval of the column densities of methane and carbon dioxide, errors in the modeled CO_2 column abundances and possible systematic differences in the light-path distribution between the two spectral fitting windows.

3.3.1. Precision Error of the Retrieval Algorithm

[23] The retrieved vertical columns exhibit a precision error in the least squares fit due to instrumental noise. The statistical fit error shows substantial variations since it strongly depends on the signal-to-noise ratio of the recorded spectra and thereby on surface albedo. On average, the standard deviation of this error term is about 1.5 and 1% for CH_4 and CO_2, respectively. Since both errors are uncorrelated, the relative uncertainty in the ratio reads

$$\sigma_{\mathrm{rel}}\left(\frac{V(\mathrm{CH_4})}{V(\mathrm{CO_2})}\right) = \sqrt{\sigma^2_{\mathrm{rel}}(V(\mathrm{CH_4})) + \sigma^2_{\mathrm{rel}}(V(\mathrm{CO_2}))}\,, \tag{4}$$

which is about 1.8% (corresponding to roughly 30 ppb) on average in our retrievals. We find typical standard deviations between modeled and measured column averaged mixing ratios of 30 ppb, being consistent with our uncertainty estimates.

[24] As single retrievals are not very precise, we rely on spatial and temporal averages that are constituted by a preferably high number of retrievals. Averaging over N independent retrievals in space and/or time, the precision error in the mean ratio reads

$$\sigma_{\mathrm{rel}}\overline{\left(\frac{V(\mathrm{CH_4})}{V(\mathrm{CO_2})}\right)} = \sqrt{\frac{\overline{\sigma^2_{rel}\left(\frac{V(\mathrm{CH_4})}{V(\mathrm{CO_2})}\right)}}{N}}. \tag{5}$$

In the following, retrieval uncertainty refers to the estimated 1-σ-error in the averaged ratio (scaled with $\overline{VMR}(CO_2)$).

3.3.2. Errors in the Modeled CO_2 Column

[25] Errors in the modeled CO_2 column and differences in the light path affect the accuracy and are harder to quantify. However, errors in the modeled CO_2 column can be assumed to be mostly well below 1%. Biomass burning events, for instance, lead to typical carbon monoxide column abundances of up to $4 \cdot 10^{18}$ molec/cm^2 in the seasonal average [*Bremer et al.*, 2004]. Assuming an emission ratio of 1:10 for carbon monoxide, the total CO_2 column would be enhanced by $4 \cdot 10^{19}$ molec/cm^2, which is only 0.5% of its background value of $8 \cdot 10^{21}$ molec/cm^2. Also strong diurnal CO_2 variations near the ground perturb

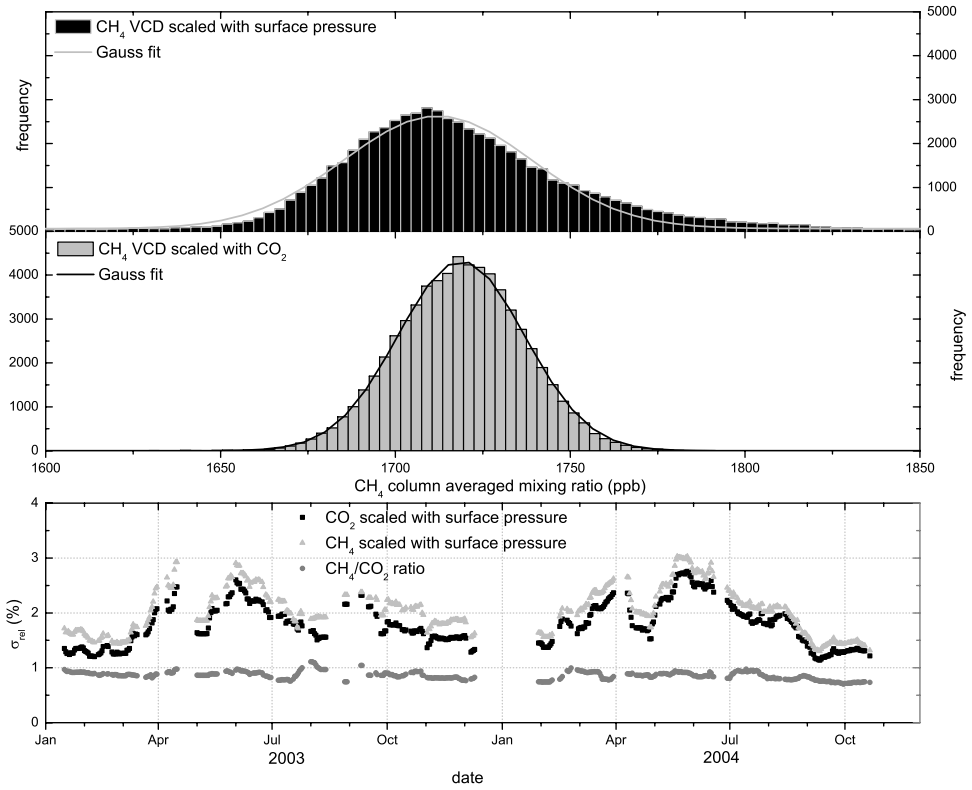

Figure 3. The effect of aerosols and clouds on SCIAMACHY retrievals over the Sahara. The upper panel shows histograms and corresponding Gaussian fits of CH_4 column-averaged concentrations over the Sahara (all retrievals from 2003 through 2004 within 20–30°N/0–20°E) derived by scaling the retrieved CH_4 VCD either by surface pressure (estimated from surface elevation, assuming a mean-sea-level pressure of 1013 hPa and an exponential pressure profile with a scale height of 8.5 km) or by the retrieved CO_2 VCD, equation (3). The lowest panel shows the standard deviation (relative in percent) of retrieved CO_2 and CH_4 VCDs scaled with surface pressure as a function of time. In addition, the relative standard deviation of the CH_4/CO_2 ratio is depicted. The same geographical area but a 30-day box filter has been used. This figure is based on all retrievals with an effective cloud-top height of less than 1 km (see text).

the total column by only 0.5% [*Olsen and Randerson*, 2004]. The strongest variations in the CO_2 column due to uptake and release mechanisms of the biosphere show a seasonal dependence and are well reproduced by the model.

3.3.3. Errors Due to Differences in the Light Path Distributions

[26] Small differences might exist between the light path distribution of the CH_4 and CO_2 retrievals, which are spectrally about 80 nm apart. These difference can be induced by changes in surface albedo, cloud albedo or aerosol optical properties.

[27] Clouds mostly shorten the light path. For cloud detection, we applied the approach of *Frankenberg et al.* [2005a], discarding measurements with an effective cloud top height (assuming that the entire ground pixel is homogeneously cloudy) of more than 1 km. Surface and cloud albedo determine which fractions of the recorded photons are scattered back from the earth's surface and cloud top, respectively (see Figure 1). If these albedos do not change between the spectral range of the two fitting windows (1563–1585 and 1631–1670 nm for CO_2 and CH_4, respectively), the light path distribution in both spectral ranges is identical. A problem arises if surface and/or cloud albedo change substantially in our wavelength range. First sensitivity studies suggest that, if cloud or surface albedo change by 25% in this spectral range, the bias could rise to ±3%, though it mostly lies between 0.5 and 2%. This potential bias increases if the cloud filter is less restrictive (e.g., allowing an effective cloud top height of 2 km) and is largest when high clouds are present.

[28] A similar consideration holds for aerosols. We analyzed retrievals over the Sahara (here: 20–30°N/0–20°E) to quantify the effect of aerosols which was found to be much larger in this region *Houweling et al.* [2005] than elsewhere. The Sahara is ideally suited for retrieval since it is mostly cloud free, exhibits a high surface albedo in the near infrared and is devoid of local methane sources. For the Sahara, we found a standard deviation of less than 10 ppb in modeled methane column abundances from January 2003 through December 2004. To analyze the effect of aerosols, we applied two approaches to convert retrieved vertical columns to column averaged mixing ratios: In the first, we scaled with the total vertical column of air (estimated from surface pressure) and in the second approach, we used concurrent CO_2 retrievals as a proxy for the probed column.

Table 2. CH_4 Emissions Applied in the TM Model

Source Category	Reference	Emission, Tg CH_4 yr^{-1}
Anthropogenic		
Domestic ruminants	EDGAR[a]	89
Fossil fuel production	EDGAR[a]	87
Waste treatment	EDGAR[a,b]	73
Rice cultivation	*Matthews et al.* [1991]	60
Biomass burning	*Olivier et al.* [2003][c]	35
Biofuel	EDGAR[a]	14
Minor sources	EDGAR[a]	5
Natural		
Wetlands	*Walter et al.* [2001][d]	155
Termites	*Sanderson* [1996]	20
Ocean	*Houweling et al.* [1999]	15
Wild animals	*Houweling et al.* [1999]	5
Volcanoes	*Houweling et al.* [1999]	4
Soil sink	*Ridgwell et al.* [1999]	−30
Total		532

[a]EDGAR version 3.2, year 1995.
[b]Landfills scaled to 40 Tg yr^{-1}.
[c]Five-year average of the period 1997–2001, with total forest burning scaled to 20 Tg yr^{-1} and savanna burning to 15 Tg yr^{-1}.
[d]Fifteen-year mean field.

[29] Figure 3 shows a histogram of the retrieved column averaged mixing ratios over the entire time period (2003–2004) using the two different approaches. It is obvious that the variations obtained using surface pressure are much larger than those obtained using CO_2 as a proxy. Also, the shape of the distribution is substantially different for both methods; using surface pressure, the distribution is not Gaussian but exhibits high frequencies at the upper tail. While clouds mostly shorten the light path, *Houweling et al.* [2005] have shown that aerosols have disparate effects on the retrieval: Depending on surface albedo and aerosol types, the light path can as well be strongly enhanced (overestimated vertical columns) as also shortened. This effect is reflected in the retrieval distribution using a simple surface pressure scaling. Most of the spread in the simple scaling approach is attributable to aerosols, clouds and, to a smaller amount, also to variations in sea level pressure and water vapor concentrations, which have not been considered in this comparison.

[30] The application of CO_2 as proxy reduces the standard deviation of the retrieved mixing ratios from 37 to 18 ppb and results in a Gaussian distribution. The effects of aerosols and clouds, uncertainties in surface pressure and water vapor column are largely eliminated. The lowest panel of Figure 3 depicts the time dependent, relative 1-σ spread of CO_2 and CH_4 VCDs scaled with surface pressure, respectively. Further, the relative spread in the ratio is shown. One can clearly see that the spread of the CH_4 and CO_2 retrievals scaled by surface pressure are correlated and exhibit substantial variations, most likely due to partial cloud cover and changes in the aerosol optical depth and height distribution (see *Houweling et al.* [2005] for a discussion on the influence of aerosols on SCIAMACHY CO_2 retrievals). The ratio of CH_4/CO_2, however, exhibits a low spread throughout the time period under consideration; The effect of aerosols is effectively neutralized in the ratio. Furthermore, the relative 1-σ spread (mostly about 0.9%) is consistent with our estimate of the retrieval precision, which is about 15 ppb over the Sahara due to the high surface albedo.

3.4. Outlook

[31] Future space missions, such as the Orbiting Carbon Observatory (OCO, Jet Propulsion Laboratory, see *Crisp et al.* [2004]) or the Greenhouse gases Observing SATellite (GOSAT, Japan Aerospace Exploration Agency), will have far smaller ground pixel sizes for which the measurement scene can be considered to be more homogenous. This should largely resolve the problem of partial cloud cover. A substantially higher spectral resolution will yield both a higher measurement precision and additional information on aerosols. Hence, these instruments are expected to facilitate the use of proxies in wavelength regions that may be spectrally distant.

4. Atmospheric Models

[32] We use two atmospheric chemistry transport models to simulate total column abundances of methane and carbon dioxide.

4.1. CH_4 Modeling With TM4

[33] The model results presented in this paper are based on simulations with the global chemistry–transport model TM4, the successor of TM3 [*Dentener et al.*, 2003, and references therein]. The model has a regular longitude–latitude spatial grid, and hybrid σ–pressure layers in the vertical. It is driven by six-hourly meteorological fields from the European Centre for Medium Range Weather Forecast (ECMWF) operational data. These fields include global distributions for horizontal wind, surface pressure, temperature, humidity, liquid and ice water content, cloud cover and precipitation. Key processes included are mass-conserved tracer advection, convective tracer transport, boundary-layer diffusion, photolysis, dry and wet deposition as well as tropospheric chemistry including non-methane hydrocarbons to account for chemical loss by reaction with OH [*Houweling et al.*, 1998]. Except for methane, anthropogenic emissions are based on *Van Aardenne et al.* [2001], which in turn is based on the widely used EDGAR (Emission Database for Global Atmospheric Research) data base [*Olivier et al.*, 1999], while natural emissions are as in *Houweling et al.* [1998].

[34] The model version employed here differs from *Dentener et al.* [2003] in a number of aspects:

[35] 1. The spatial resolution is 3 × 2 degrees, with 25 vertical levels up to 0.1 hPa.

[36] 2. A mass-conserving pre-processing of the meteorological input is applied according to *Bregman et al.* [2003].

[37] 3. The stratospheric destruction of methane by reaction with OH, Cl and $O(^1D)$ is taken into account by applying correction factors to the model-calculated destruction rate based on a 2D-model (G. Velders, personal communication).

[38] 4. Furthermore, CH_4 concentrations above 50 hPa are nudged to the monthly-mean zonal HALOE/CLAES climatology from UARS [*Randel et al.*, 1998].

[39] 5. The emissions of methane are as described in Table 2. Modifications with respect to *Frankenberg et al.*

[2005a] are: (1) EDGAR version 3.2 is used instead of 2.0; (2) biomass burning emissions are based on *Olivier et al.* [2003] instead of *Hao et al.* [1991]; (3) emissions have been scaled to different global totals for a number of source categories, most notably total rice emissions have been reduced from 80 to 60 Tg yr^{-1}, in agreement with *Olivier et al.* [1999].

[40] The model has been run for the period 2000 through 2004. The simulated methane burden is approximately in steady-state at 4850 Tg during this period, with a tropospheric (below 100 hPa) lifetime of around 9.4 years. Modeled concentrations are generally in good agreement with surface measurements from the NOAA-CMDL network [e.g., *Dlugokencky et al.*, 2003], although the interpolar difference is overestimated by around 30 ppb. So far, it is unclear whether these discrepancies are due to errors in transport, OH fields or emission inventories.

4.2. CO_2 Modeling With TM3 3.8

[41] TM3-MPI 3.8 *Heimann and Körner* [2003] is a three-dimensional global atmospheric transport model for an arbitrary number of active or passive tracers. In this study, we use meteorological reanalysis fields from the National Centre for Environmental Prediction (NCEP/DOE AMIP-II). The model was run with a resolution of $1.8^\circ \times 1.8^\circ$ and 28 height layers. The ocean as source or sink for atmospheric CO_2 was implemented according to *Takahashi et al.* [2002] using monthly mean fluxes without interannual variations. Anthropogenic emissions are derived from the EDGAR 3.2 database [*Olivier and Berdowski*, 2001] by temporal extrapolation of the annual mean fluxes of 1990 and 1995. Those mainly include agricultural activities and biomass burning. The CO_2 fluxes from the natural biosphere were modeled by the BIOME-BGC ecosystem model using the same temporally resolved meteorology as the atmospheric transport. The biosphere fluxes follow a diurnal cycle. To obtain realistic spatial gradients, the model was run over a spin-up time of 10 years with a coarser resolution, starting from a globally constant CO_2 mixing ratio. The years 2002 and 2003 were modeled with the final resolution.

[42] Verification of the transport properties of the model was performed by *Heimann and Körner* [2003]. Especially for CO_2, comparison of TM3 results with in-situ atmospheric measurements from various aircraft campaigns and ground based measurements shows that the model simulates realistic mixing ratio distributions not only at the surface but also in upper parts of the troposphere (Peylin et al., LSCE Paris, manuscript in preparation).

[43] So far, only model results of the year 2003 were applied. These were also used for the correction of the seasonal CO_2 variations in 2004.

4.3. Comparing Models With SCIAMACHY Retrievals

[44] The atmospheric models provide mixing ratios in different height layers. These can be converted to the vertical column of each height layer (V_i). In principle, the (mass weighted) column averaged mixing ratio of the model output could then be computed as the ratio of the sum of all vertical sub-columns of the trace gas species of interest to the total vertical column of all atmospheric constituents. For comparison of model output to SCIAMACHY measurements, this simple approach is no more valid as it does not take instrument sensitivity into account. The averaging kernels (Figure 2) show that perturbations, especially in higher atmospheric layers, are generally underestimated by the SCIAMACHY retrieval by up to 50%. In order to have a comparable modeled mixing ratio, the model output has to be converted to the column averaged mixing ratio that SCIAMACHY would measure if the model represented the exact methane profile. This conversion has been applied to the modeled methane abundances using equation ak1, a considerable improvement to *Frankenberg et al.* [2005a] where the modeled column averaged mixing ratios were computed without taking instrument sensitivity into consideration.

[45] The basic effect of this conversion is that perturbations in the model from the a priori sub-column are damped by the factor given in the averaging kernel at the respective height. Thus, the strongest effect of this conversion to SCIAMACHY sensitivity is to curb stratospheric methane variations. In most cases, tropical regions exhibit higher methane mixing ratios (compared to the a priori level) in the upper troposphere and lower stratosphere (UTLS), whereas polar regions show lower abundances (see stratospheric methane climatology from the HALOE instrument on board the UARS satellite: http://haloedata.larc.nasa.gov/home/index.php). Adjusting column averaged mixing ratios derived from the model to SCIAMACHY sensitivity thus implies a reduction in the tropics and an increase in polar regions (compared with a simple computation of the modeled column averaged mixing ratios).

[46] When interpreting the results presented in this study, care has to be taken not to confuse column averaged mixing ratios with tropospheric or even surface mixing ratios. Since methane is depleted in the stratosphere, the VMRs presented in this study are generally lower than pure tropospheric mixing ratios.

5. Results

[47] We present the column averaged mixing ratios of methane as a 2-year average as well as seasonal averages.

5.1. Two-Year Average Maps of Methane Abundances

[48] Figure 4a depicts the two-year average VMR of methane. A simple cloud filter discarding retrievals with an effective cloud top height of over 1 km was applied. The overall variations are rather small, most deviations from the global mean being well below 5%. The most striking feature is the clear north-south gradient caused by higher natural and anthropogenic methane emissions in the northern hemisphere. The entire Australian continent as well as southern parts of Africa and South America show very low methane abundances compared to the mid-latitudes. Moreover, there is little scatter on smaller scales, i.e., most pixels show a strong spatial correlation to surrounding areas. This is mostly due to the relatively long lifetime of methane, leading to extended areas of enhancement even for point sources. We restrict the long-term average plots to landmasses since a reasonable retrieval over the ocean requires either low lying clouds, sun glint or a very rough ocean surface to exhibit a sufficiently high albedo. Thus, long-term maps over the ocean would be strongly biased to

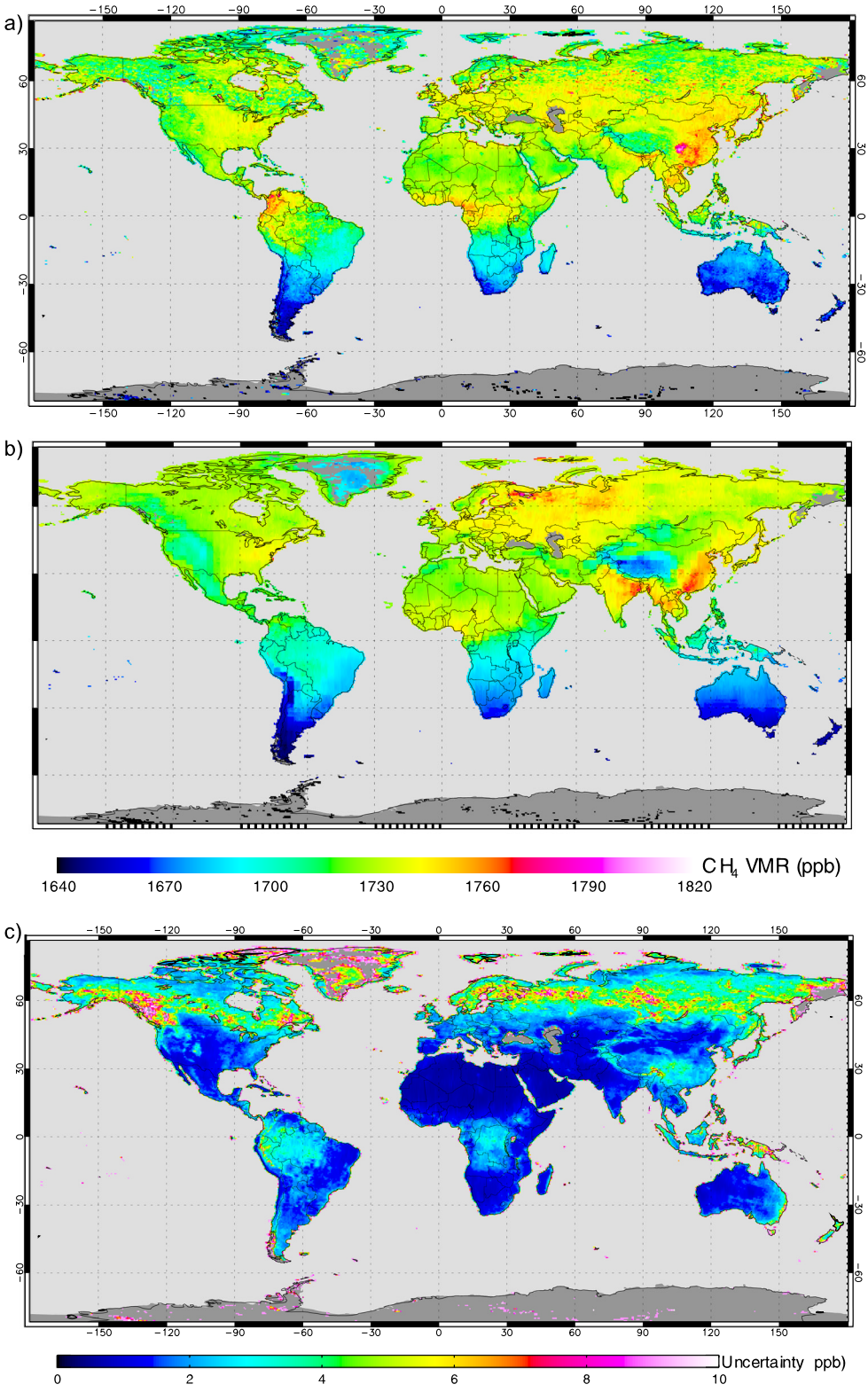

Figure 4. (a) Two-year average of column averaged mixing ratios (in ppb) of methane retrieved from SCIAMACHY from January 2003 through December 2004. The measurements have been gridded with a spatial resolution of 0.5° longitude times 0.5° latitude. (b) Corresponding (i.e., sampled at the exact place and time of the measurements) TM4 model results. (c) Estimated statistical uncertainty associated with the SCIAMACHY retrieval (see section 3.3 for details).

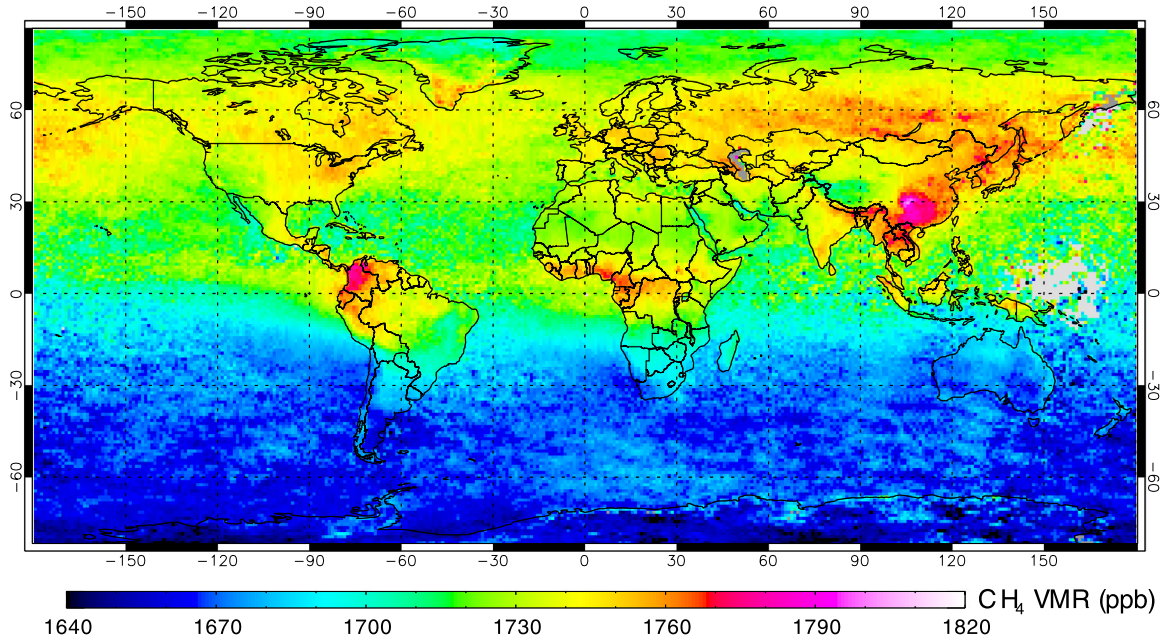

Figure 5. Two-year average of methane VMR as retrieved by SCIAMACHY with less strict cloud filter (effective cloud top height less than 2.5 km) and gridded on 1° longitude times 1° latitude.

certain seasons. In addition, the statistical uncertainties (1-σ) in the SCIAMACHY averages (as defined in section 3) are shown in Figure 4c. Higher uncertainties are mainly due to low sampling frequency or low surface albedo (e.g., parts of Russia and Canada as well as retrievals at coastlines). Figure 4b shows the corresponding TM4 model output. Both the north-south gradient and the main regions with enhancements predicted by the model are on the whole consistent with the measurements. In northern South America and central Africa, however, the retrievals reflect higher methane abundances than the model. As already mentioned, disparities in the light path due to high-frequency spectral structures in surface or cloud albedo are a possible source of bias. This bias would therefore also depend on the surface type and albedo. However, there is no indication for such behavior in the two-year average: The retrievals vary smoothly over different surface types.

[49] Figure 5 depicts the same SCIAMACHY retrievals as in Figure 4a but with a less strict cloud filter (effective cloud top height below 2.5 km) and without discarding retrievals over the ocean. Thereby we achieve full global coverage. The north-south gradient can also be well observed over the ocean. Most methane abundances, surprisingly, are higher than in Figure 4a. However, the absolute values have to be interpreted with care because, as discussed in section 3, clouds are a potential source of bias, especially if no strict cloud filter is applied. At the continent-ocean border, the frequency of reasonable retrievals changes abruptly (less reliable measurements over the ocean), often resulting in a rather steep gradient in the observed mean of methane abundances. We see that clouds do not always hinder a reasonable retrieval, contributing, on the contrary, to meaningful measurements if a suitable proxy for the light-path is applied. In the future, the combination of information on effective cloud top height and cloud fraction as well as surface and cloud albedos will facilitate the quantification of the effect of clouds. At present, we minimize the errors induced by partial cloud cover by confining our analysis to retrievals that comply with the strict cloud filter criteria.

[50] In Figure 4a, various regions with enhanced methane abundances (on larger spatial scales) can be detected. Retrieved VMRs in Russia show substantial variation and are hard to interpret due to the absence of strong spatial correlation of high methane abundances to surrounding pixels and a relatively high uncertainty in the retrievals (mostly due to low surface albedo, see Figure 4c). Thus, we focus on regions where uncertainties in the average are low and signals from methane emissions strong.

[51] There are regions with substantially enhanced CH_4 VMRs indicating strong regional methane emissions. The most outstanding region is the Red Basin in China showing the highest mean abundances on the entire globe (please note that the highest values are depicted in white). Further, there are high VMRs in northern parts of South America (not in line with the modeled abundances in Figure 4a), central Africa and also slight enhancements in the U.S.A.. A zoom into these regions with a narrower color-scale is shown in Figure 6.

[52] In the United States (Figure 6a), the highest abundances are observed south of the Great lakes. According to the EDGAR base [*Olivier and Berdowski*, 2001], emissions from coal mining are very strong in this regions, but other anthropogenic activities also play a significant role. The Rocky mountains show lower VMRs partly due to high surface elevation that results directly in a reduced column averaged VMR (due to the relatively stronger weight of the stratosphere in case of low surface pressure). Also, this region exhibits few sources of methane. Strong variations in coastal areas may be related to an overall higher

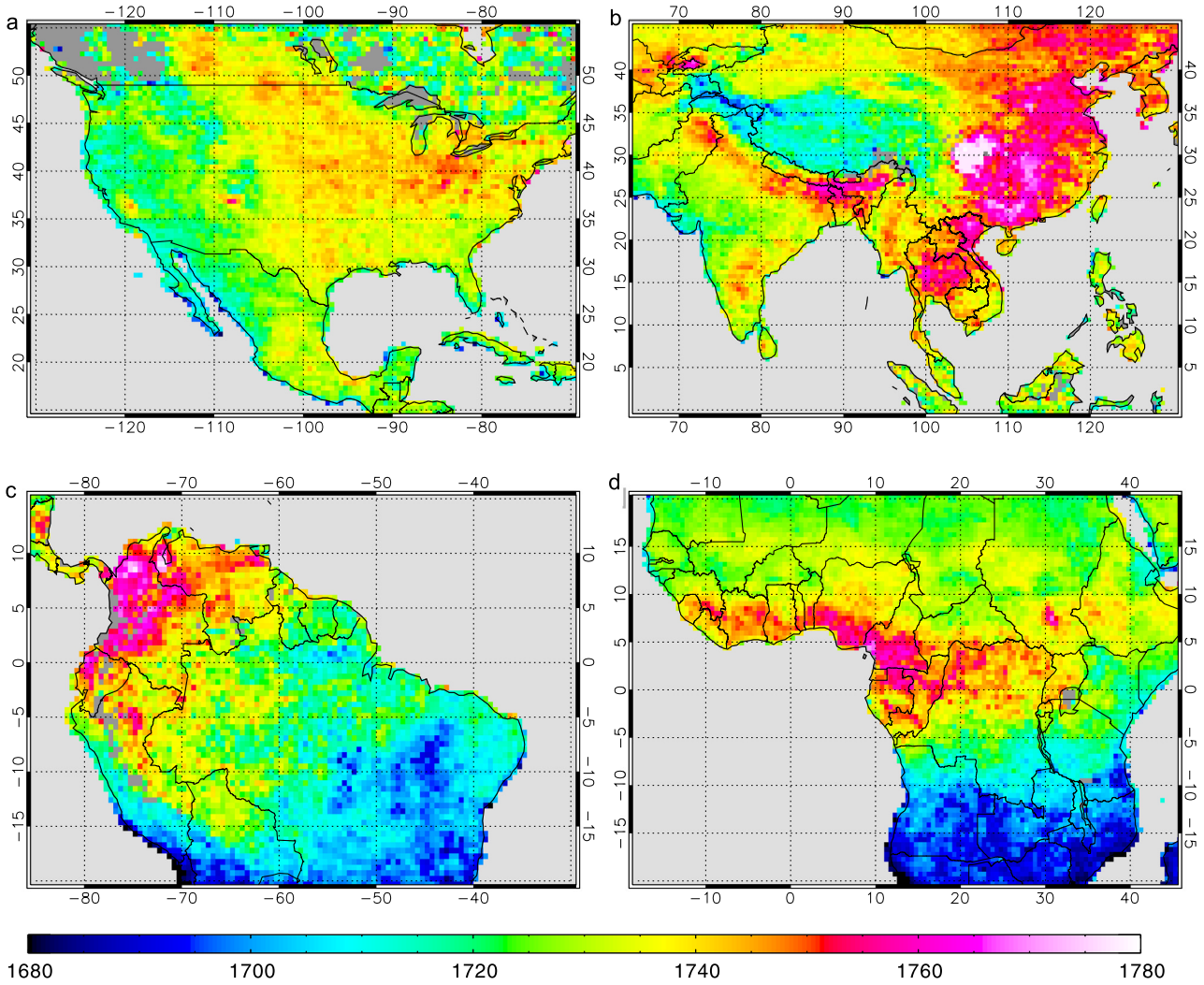

Figure 6. Global methane mean column averaged mixing ratios (in ppb). The same time period and spatial resolution as in Figure 4a is used but with a different color scale and with focus on four specific geographical regions, namely, (a) United States, (b) Asia, (c) South America, and (d) Africa. Note that the highest abundances are shown in white whereas pixels with missing data (e.g., over ocean) are shown in gray. Only pixels with a maximum statistical error of 8 ppb are depicted.

uncertainty in the averaged mixing ratios in these regions (see Figure 4c) due to lower albedos or a smaller number of measurements within these pixels. The same could hold for the peculiar enhancement in New Mexico at approximately 36.75°N and 108°W, but further investigations are necessary to ascertain the cause of the enhancement.

[53] In Asia (Figure 6b), the highest methane abundances by far are found, particularly in the Red Basin (major cities: Chengdu and Chongqing) and regions further south-east. Rice paddies, coal mining, domestic ruminants and waste handling can be assumed to constitute the main sources. In India, the entire Gangetic plains (rice paddies, domestic ruminants) show higher methane VMRs than the surrounding areas. Also in Thailand, Laos and Vietnam, substantial enhancements are observed. Inverse modeling is required to attribute the emissions quantitatively to different sources. In Southeast Asia, rice paddies, wetlands, landfills and domestic ruminants are the strongest sources according to *Olivier and Berdowski* [2001].

[54] In South America (Figure 6c), the highest abundances are found in Venezuela (close to Lake Maracaibo), Columbia, Ecuador and parts of Peru. Also parts of Brazil in the Amazon basin show high VMRs. Particularly surprising are the high values in Venezuela and Columbia: The observed VMRs are much higher than those modeled by TM4 (based on the emission inventories in Table 2). In Colombia, the major part of emissions is supposed to be attributable to digestive processes of dairy and meat cattle [*Gonzalez and Rodriguez*, 2000; *Olivier and Berdowski*, 2001]. However, these sources are not expected to exhibit the strong seasonal variations that we observe in methane abundances over Colombia (see section 5.2). One might argue that high CH_4 concentrations may be transported into this region. However, the effect of emissions on atmospheric concentrations would be expected to diminish away from source regions. Since the CH_4 abundances are highest in Colombia/Venezuela, they have to be caused mainly by

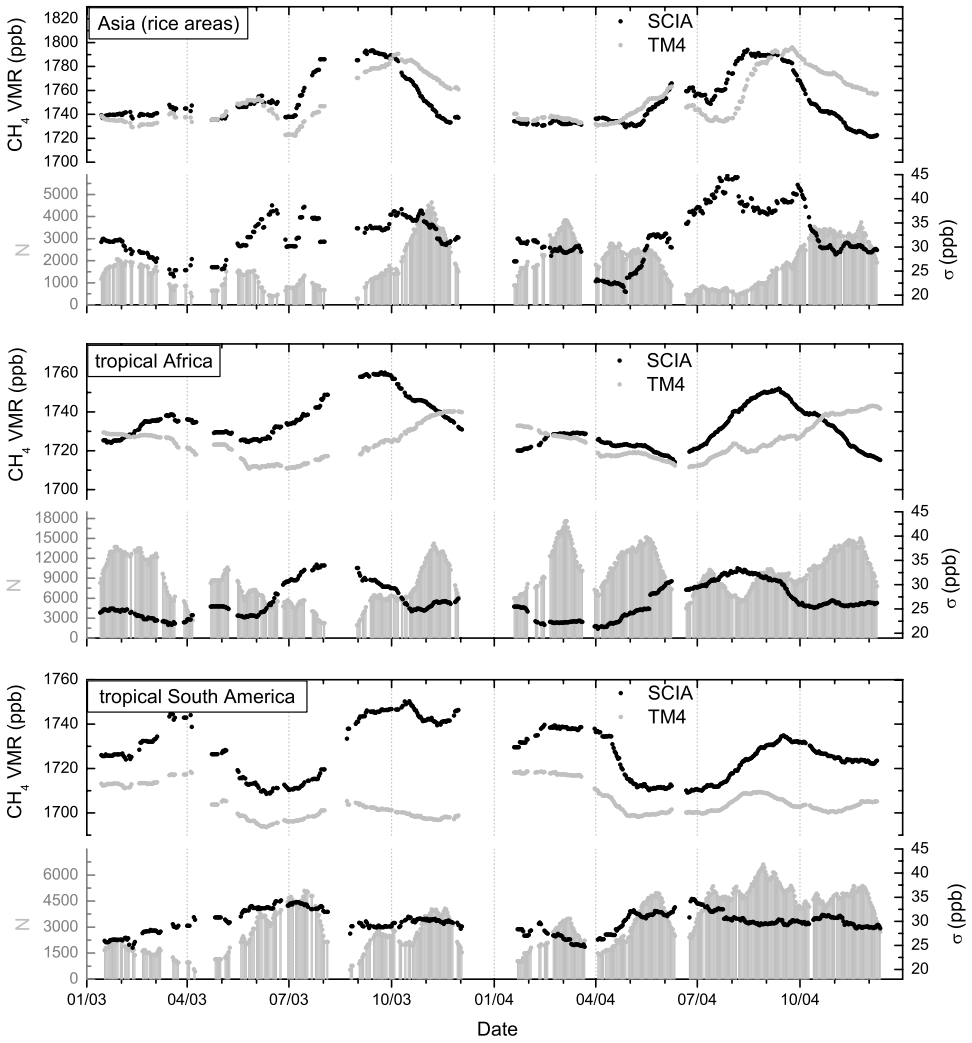

Figure 7. Time series of SCIAMACHY measurements in different geographic locations smoothed in time with a 30 day box filter (±15 days). In the upper panels, the SCIAMACHY retrieval (corrected with model CO_2 fields) and the TM4 model results (using averaging kernel correction) are depicted. The respective bottom panels show the total number of SCIAMACHY retrievals (in gray) and their standard deviation (black dots, not to be confused with the 1-σ precision error) as used for the calculation of the 30-day running average. For the averaging, only retrievals in areas with less than 1 km surface elevation are considered. The exact geographic locations of the areas are 20–30°N/80–120°E for Asia, 10°S–15°N/20°W–60°E for tropical Africa and 10°S–15°N/40–90°W for tropical South America. Gaps in the time series are caused by missing SCIAMACHY data and the cloud filter (not all SCIAMACHY data were available and due to the ice layer on channels 7 and 8, SCIAMACHY switches to the decontamination mode from time to time).

local emissions, while transport can only explain part of the enhancements.

[55] In Africa (Figure 6d), rather homogenous enhancements between 4°S and 8°N (west of 40°E) are found. Below 8°S, methane is clearly depleted. In Sudan, a region with distinctively high methane emissions from wetlands is apparent in the SCIAMACHY retrievals as predicted by wetland models [*Walter et al.*, 2001]. Surprisingly, on the other hand, there are also enhanced VMRs in Ethiopia.

5.2. Seasonal Variations in Global Methane Abundances

[56] Seasonal variations in methane abundances may be induced due to several factors apart from emissions with strong seasonal patterns such as rice emissions or biomass burning. Variations in predominant wind fields caused by ITCZ movements, for instance, or changes in OH fields can also cause strong seasonal variations in methane abundances. For a first quantitative analysis of the time dependence of the methane distribution, we developed time series in different geographic locations. For the SCIAMACHY retrieval and the TM4 model results, we applied a 30 day box filter (±15 days) to smooth the data. In Figure 7, the temporal behavior over Asia (20–30°N/80–120°E), tropical Africa (10°S–15°N/20°W–60°E) and tropical South America (10°S–15°N/40–90°W) are shown. In Asia, the main seasonality is caused by rice emissions, which are very intense during a relatively short time period. As can be seen

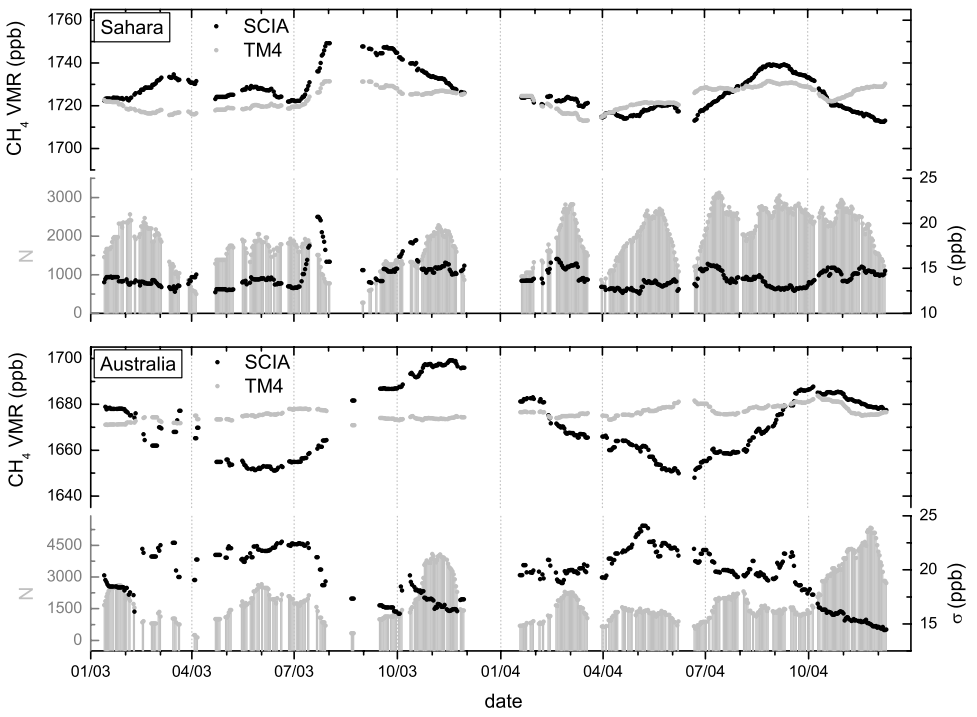

Figure 8. Time series of SCIAMACHY measurements over the Sahara and Australia. The same criteria as in Figure 4 apply. The exact geographic locations of the areas are 20–30°N/0–20°E for the Sahara and 20°–30°S for the complete Australian continent. The latitudinal bins have been chosen to have comparable solar zenith angles (with a phase shift of 6 months) for both regions. The respective bottom panels depict the total number of SCIAMACHY retrievals and their standard deviation as used for the calculation of the 30-day running average.

in the upper panel of Figure 7, methane enhancements due to rice emissions (peak months are August through October) seem to occur approximately 1 month earlier than given in the model, although the magnitude is very similar (given 60 Tg yr^{-1} rice emissions in the model). Higher methane abundances are also seen to decline earlier, resulting in markedly lower SCIAMACHY retrievals in November as compared to the model. These results are consistent with the findings of *Chen* [2003] who also found a time shift in methane emissions with respect to current emission inventories. The start of the rice emissions is also reflected in an enhanced standard deviation of the SCIAMACHY retrievals since local sources induce large scatter.

[57] Especially for modeling purposes, the temporal evolution of sources is of primary importance. These emissions largely determine methane abundances in the entire Asian region and are also transported towards Africa [*Frankenberg et al.*, 2005a] or North America. Different regions can be affected depending on predominant wind fields during the time of peak emissions.

[58] Also in tropical Africa, we observe a phase shift between SCIAMACHY retrievals and model simulations. The absolute abundances are in general on the same order but the measurements show higher mixing ratios starting already in July/August. In tropical South America, measurements are higher than the model throughout the year. However, as in *Frankenberg et al.* [2005a], the largest discrepancies are found from August through December, especially in 2003. For the rest of the year, the temporal evolution of measurement and model is very similar apart from an offset of ≈15–30 ppb at any given time. Part of the seasonality, such as the decline in methane abundances after April, is due to movements of the ITCZ. August through September is the typical biomass burning season in tropical South America as is evident in observations of increased carbon monoxide abundances [*Bremer et al.*, 2004; *Frankenberg et al.*, 2005c]. Depending on vegetation and fire type, molar emission ratios (CH_4/CO_2) of biomass burning range from 0.4% to 1.3% [*Andreae and Merlet*, 2001] with indications of even higher ratios in tropical rainforest areas [*Alvala and Kirchhoff*, 1998]. If the emission ratio of methane is exactly the same as the ratio of the background concentrations (≈0.5%), the methane emissions would be indiscernible to us if the particular biomass burning event is not correctly included in the CO_2 model. Thus, biomass burning can be a source

Figure 9. Seasonal plots (December/January/February, March/April/May, June/July/August and September/October/November) as retrieved by SCIAMACHY in the the years 2003 and 2004 (averaged over 1° longitude and 1° latitude). For comparison, the TM4 model results for the same time periods are depicted on the right-hand side. Only pixels with an estimated statistical error of less than 15 ppb are depicted. The statistical retrieval uncertainties in the SCIAMACHY averages are shown in the lower panels (Figures 9i–9l).

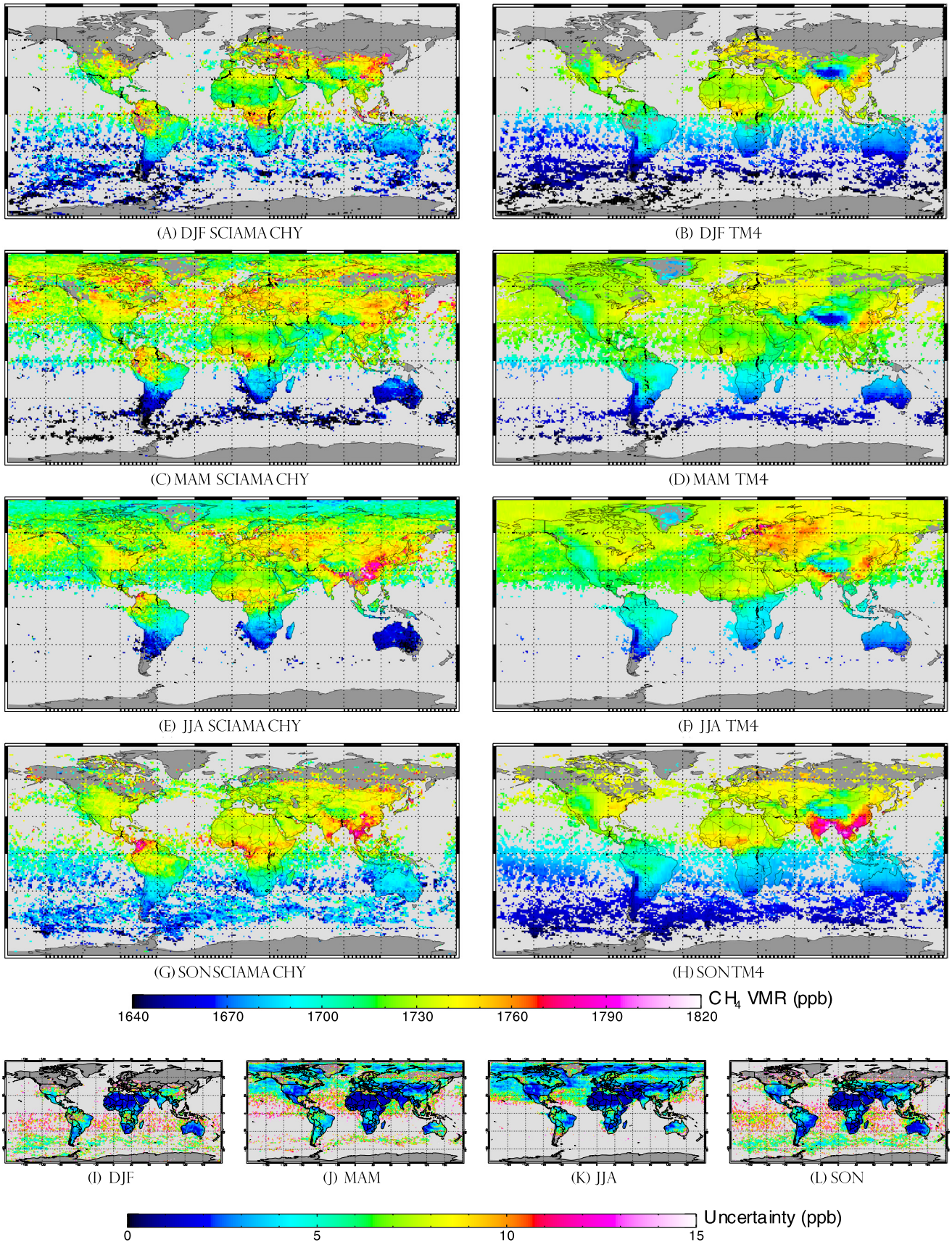
(A) DJF SCIAMACHY
(B) DJF TM4
(C) MAM SCIAMACHY
(D) MAM TM4
(E) JJA SCIAMACHY
(F) JJA TM4
(G) SON SCIAMACHY
(H) SON TM4
CH4 VMR (ppb)
1640
1670
1700
1730
1760
1790
1820
(I) DJF
(J) MAM
(K) JJA
(L) SON
Uncertainty (ppb)
0
5
10
15

Figure 9

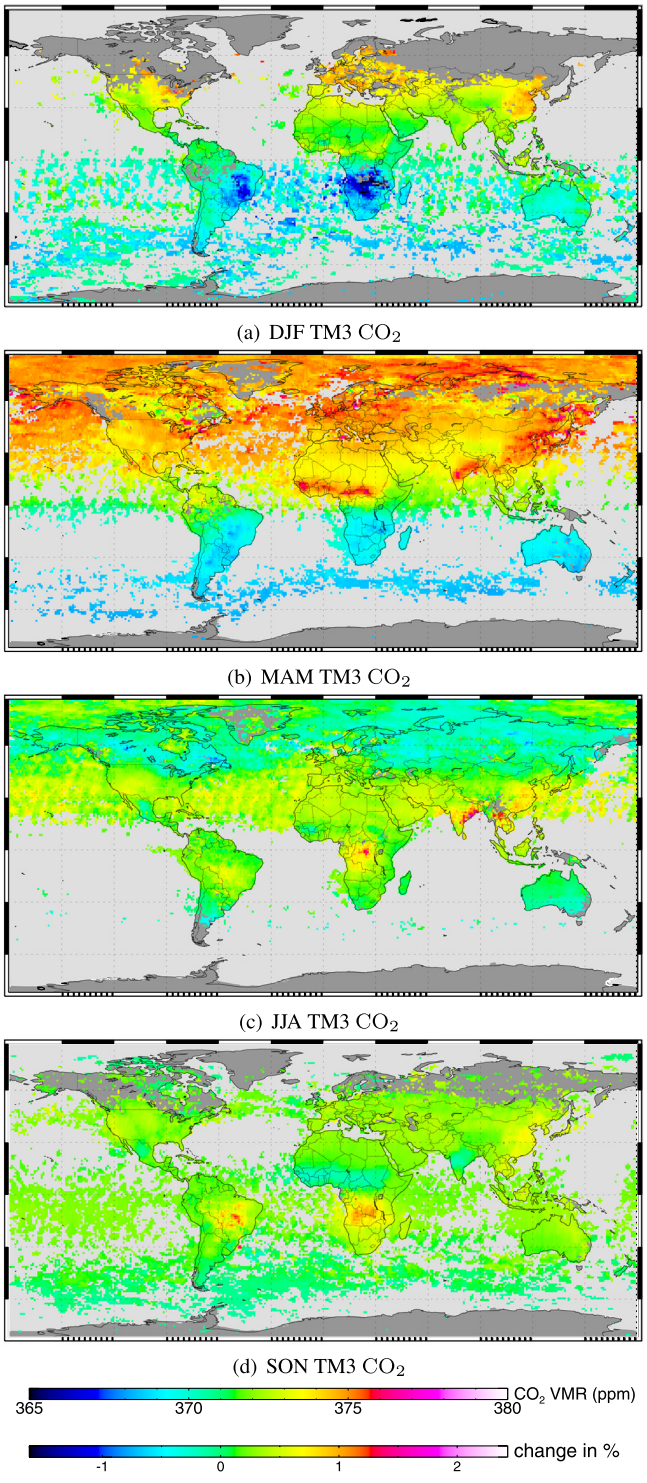

Figure 10. Seasonal plots (December/January/February, March/April/May, June/July/August and September/October/November, derived from TM3-MPI) of the modeled column averaged CO_2 mixing ratio as used for the calculation of the mixing ratio of CH_4.

of differences between model and measurements, especially in direct proximity of the fires.

[59] Figure 8 shows time series for the Sahara and Australia. In general, the retrieval over the Sahara does not show large discrepancies compared to the model. Both capture enhanced methane abundances starting in July 2003 but with a higher magnitude in the measurement. These enhancements are accompanied by a relatively high standard deviation in the measurements. Because of the lack of local sources, this suggests that the enhancements are induced by transport, either from Europe or from Asia.

[60] In Australia, there are systematic differences between model and measurement. The SCIAMACHY retrieval shows seasonal variations that are not predicted by the model. The model simulations show close agreement with NOAA-CMDL surface measurements at Cape Grim, Samoa and Easter Island, and are also consistent with FTIR CH_4 column measurements at Wollongong [*Dils et al.*, 2005]. The sinusoidal variations in time have a minimum in June and a maximum in December, albeit with a relatively low amplitude (±1.2%). A retrieval dependence on solar zenith angle cannot explain the variations as this should result in a similar behavior over the Sahara (with a 6-month phase shift), which is not the case (Figure 8). Potential alternative explanations are unaccounted variations in CO_2 or a hitherto unknown retrieval bias.

[61] A global view of the seasonal cycle gives a better overview of the seasonal cycles in different geographic locations. Figure 9 shows seasonal plots of retrieved and simulated global methane VMRs.

[62] The associated CO_2 model fields that were used for the computation of methane column averaged mixing ratios are depicted in Figure 10. It should be noted that the retrievals in the seasonal mean are sometimes only single snapshots of the methane distribution. Especially over the ocean, only few valid measurements are available due to the low ocean albedo in the near infrared, causing, in most cases, an unacceptably reduced signal-to-noise ratio. Hence, care has to be taken in interpreting the seasonal means and, the 1-σ uncertainties given in Figures 9i–9l have to be considered. Enhanced methane VMRs south of Iceland appear in the June/July/August average. From the model simulation we could infer that the enhancement is largely due to a transport event on 18–20 July 2003.

[63] The most pronounced feature we observe is due to the temporal variation of methane emissions from rice paddies in Southeast Asia with typical maxima from August through October, resulting in higher VMRs in the periods June–August and September–November. The differences between model and measurement in this case partly result from the deviation of the observed from the modeled temporal evolution (see Figure 7). In Africa, the highest methane abundances are situated towards the south in Dec/Jan/Feb, while they are strongest and situated further northward in Sep/Oct/Nov. This, on the whole, corresponds well to the temporal evolution and spatial distribution of wetland emissions [*Shindell et al.*, 2004].

[64] In South America, the highest abundances are found from January through April, in line with current wetland distributions. However, in northern parts of South America the highest abundances appear from September through November, as also evident in the two-year mean (see Figure 6c). The current emission inventory for Colombia and Venezuela (together 4.9 Tg yr^{-1} given by the EDGAR (Emission Database for Global Atmospheric Research) database [*Olivier and Berdowski*, 2001]) can hardly explain

such abundances. The seasonality of the signal calls for an exclusion of more or less constant sources such as energy related emissions or cattle breeding. The total rice production in Colombia is only 2% of that in India (see Food and Agriculture Organization of the United Nations, http://apps.fao.org) and thus unlikely to be the source of such high methane abundances. Other possible tropical sources are biomass burning and termites. However, in northern South America no substantial biomass burning was detected in the July–November period (*Bremer et al.* [2004], Tropospheric Emission Monitoring Internet Service, http://www.temis.nl), while termites are not expected to exhibit strong seasonality in their methane emissions [*Zimmermann et al.*, 1982; *Sanderson*, 1996]. Thus, the origin of these high abundances still remains unclear.

[65] A more detailed discussion and rigorous comparison with atmospheric models using different emission inventories will be presented in a subsequent publication (P. Bergamaschi et al., manuscript in preparation, 2006).

6. Conclusions

[66] The space-borne spectrometer SCIAMACHY on board ENVISAT now enables first precise measurements of atmospheric methane from space with high sensitivity including toward the ground and global coverage over continents. In this paper, we investigate available SCIAMACHY data in the years 2003 and 2004 and derive maps of the methane distribution as well as the corresponding methane abundances modeled with the atmospheric chemistry transport model TM4. We use CO_2 as a proxy for the probed atmospheric column to convert methane total columns to column averaged mixing ratios. For this purpose, concurrent retrievals of the total column of CO_2 are used in combination with modeled CO_2 abundances. Since variations in the CO_2 column abundances are far smaller than those in methane, we retrieve precise maps of the column averaged mixing ratio of methane.

[67] In these maps, the north-south gradient can be clearly identified. In the two-year average, we found the most pronounced enhancements of methane in the Red Basin of China and in large areas of Asia in general, followed by northern parts of South America and central Africa. In particular, the high mixing ratios in Columbia and Venezuela are surprising, and much higher than our TM4 simulations. This indicates higher CH_4 emissions in this region than given by the CH_4 inventories used in our study. The largest seasonal variations are caused by rice emissions in Asia, which are very intense during a relatively short time period. Our measurements indicate that these emissions already start towards the end of July and decline sharply in November, which is earlier than predicted by the model based on the inventory by *Matthews et al.* [1991]. This is of primary importance for the modeling of global methane abundances.

[68] Confirming our previous analysis [*Frankenberg et al.*, 2005a], we found strong deviations between observed and modeled CH_4 abundances in tropical regions, hinting at so far underestimated tropical emissions. The analysis of the two-year period reveals that these discrepancies between measurements and model are highest in the time period from August through December, especially in the year 2003.

[69] Over Australia, we found unexpected seasonal variations ($\pm 1.2\%$) in the measured CH_4/CO_2 ratio. To date, the origin of this behavior remains unclear and needs further investigations to exclude a measurement bias.

[70] In the long term, however, the correlation with atmospheric models is very good and the standard deviation between model and measurement is about 30 ppb [*Frankenberg et al.*, 2005a], which corresponds to a retrieval precision of 1.8% for a single measurement. Thus, the measurements represent an enormous potential for verifying or correcting current methane emission inventories. A more detailed comparison with the atmospheric models TM4 and TM5 [*Krol et al.*, 2005], including the analysis of different emission inventories and application of high-resolution atmospheric models [*Krol et al.*, 2005; *Bergamaschi et al.*, 2005] for source regions of special interest, will be part of a subsequent publication (P. Bergamaschi et al., manuscript in preparation, 2006).

[71] **Acknowledgments.** Most importantly the authors would like to thank all scientists and engineers involved in the European Space Agency's ENVISAT/SCIAMACHY mission, especially John Burrows and his team from the University of Bremen. If they had not fought shadows, SCIAMACHY would not have been possible. We also thank the national space agencies of Germany (DLR), the Netherlands (NIVR) and Belgium (BUSOC). The SCIAMACHY level-1 data used in this paper were made available by ESA and processed by DLR. We thank the Netherlands SCIAMACHY Data Center, in particular Ankie Piters and John van de Vegte from KNMI, for their invaluable assistance in transferring the data set to Heidelberg. We thank Tim Deutschmann for writing C libraries to access SCIAMACHY data and Suniti Sanghavi for proofreading the manuscript. We wish to acknowledge the European Commission for supporting the 5th Framework Programme RTD project EVERGREEN (contract number EVG1-CT-2002-00079). We further acknowledge exchange of information within the EU 6th FP Network of Excellence ACCENT (http://www.accent-network.org/).

References

Alvala, P., and V. Kirchhoff (1998), Observations of atmospheric methane and carbon monoxide in Brazil: SCAR-B mission, *J. Geophys. Res.*, *103*(D24), 31,101–32,105.

Andreae, M., and P. Merlet (2001), Emission of trace gases and aerosols from biomass burning, *Global Biogeochem. Cycles*, *15*, 955–966.

Bergamaschi, P., M. Bräunlich, T. Marik, and C. Brenninkmeijer (2000), Measurements of the carbon and hydrogen isotopes of atmospheric methane at Izaña, Tenerife: Seasonal cycles and synoptic-scale variations, *J. Geophys. Res.*, *105*(D11), 14,531–14,546.

Bergamaschi, P., H. Behrend, and A. Jol (2004), Inverse modelling of national and EU greenhouse gas emission inventories - Report of the workshop "Inverse Modelling for Potential Verification of National and EU Bottom-Up GHG Inventories" under the mandate of the Monitoring Mechanism Committee WG-1 23–24 October 2003, Joint Res. Cent., Ispra, Italy.

Bergamaschi, P., M. Krol, F. Dentener, A. Vermeulen, F. Meinhardt, R. Graul, M. Ramonet, W. Peters, and E. J. Dlugokencky (2005), Inverse modelling of national and European CH_4 emissions using the atmospheric zoom model TM5, *Atmos. Chem. Phys. Discuss.*, *5*, 1007–1066.

Bovensmann, H., J. P. Burrows, M. Buchwitz, J. Frerik, S. Noël, V. V. Rozanov, K. V. Chance, and A. Goede (1999), SCIAMACHY - Mission objectives and measurement modes, *J. Atmos. Sci.*, *56*, 127–150.

Bregman, B., A. Segers, M. Krol, E. Meijer, and P. van Velthoven (2003), On the use of mass-conserving wind fields in chemistry–transport models, *Atmos. Chem. Phys.*, *3*, 447–457.

Bremer, H., J. Kar, J. R. Drummond, F. Nichitu, J. Zou, and J. Liu (2004), Spatial and temporal variation of MOPITT CO in Africa and South America: A comparison with SHADOZ ozone and MODIS aerosol, *J. Geophys. Res.*, *109*, D12304, doi:10.1029/2003JD004234.

Buchwitz, M., and J. Burrows (2003), Retrieval of CH_4, CO, and CO_2 total column amounts from SCIAMACHY near-infrared nadir spectra: Retrieval algorithm and first results, in *Remote Sensing of Clouds and*

the Atmosphere VIII, edited by K. Schfer, A. Comeron, M. Carleer, and R. Picard, *Proc. SPIE*, *5235*, 375–388.

Buchwitz, M., V. Rozanov, and J. Burrows (2000), A near-infrared optimized DOAS method for the fast global retrieval of atmospheric CH_4, CO, CO_2, H_2O, and N_2O total column amounts from SCIAMACHY Envisat-1 nadir radiances, *J. Geophys. Res.*, *105*(D12), 15,231–15,245.

Buchwitz, M., R. Beek, K. Bramstedt, S. Noël, H. Bovensmann, and J. Burrows (2004), Global carbon monoxide as retrieved from SCIAMACHY by WFM-DOAS, *Atmos. Chem. Phys. Discuss.*, *4*, 2805–2837.

Buchwitz, M., et al. (2005a), Atmospheric methane and carbon dioxide from SCIAMACHY satellite data: Initial comparison with chemistry and transport models, *Atmos. Chem. Phys.*, *5*, 941–962.

Buchwitz, M., R. de Beek, S. Noel, J. Burrows, H. Bovensmann, H. Bremer, P. Bergamaschi, S. Koerner, and M. Heimann (2005b), Carbon monoxide, methane and carbon dioxide columns retrieved from SCIAMACHY by WFM-DOAS: Year 2003 initial data set, *Atmos. Chem. Phys. Discuss.*, *5*, 1943–1971.

Burrows, J. P., et al. (1999), The Global Ozone Monitoring Experiment (GOME): Mission concept and first scientific results, *J. Atmos. Sci.*, *56*, 151–175.

Butler, T. M., I. Simmonds, and P. J. Rayner (2004), Mass balance inverse modelling of methane in the 1990s using a chemistry transport model, *Atmos. Chem. Phys.*, *4*, 2561–2580.

Chen, Y.-H. (2003), Estimation of methane and carbon dioxide surface fluxes using a 3-D global atmospheric chemical transport model, *Tech. Rep. 73*, Cent. for Global Change Sci., Dep. of Earth, Atmos., and Planet. Sci., Mich.

Clerbaux, C., J. Hadji-Lazaro, S. Turquety, G. Mégie, and P.-F. Coheur (2003), Trace gas measurements from infrared satellite for chemistry and climate applications, *Atmos. Chem. Phys.*, *3*, 1495–1508.

Crisp, D., et al. (2004), The Orbiting Carbon Observatory (OCO) mission, *Adv. Space Res.*, *34*(4), 700–709.

Dentener, F., M. van Weele, M. Krol, S. Houweling, and P. van Velthoven (2003), Trends and inter-annual variability of methane emissions derived from 1979–1993 global CTM simulations, *Atmos. Chem. Phys.*, *3*, 73–88.

Dentener, F., D. Stevenson, J. Cofala, R. Mechler, M. Amann, P. Bergamaschi, F. Raes, and R. Derwent (2005), The impact of air pollutant and methane emission controls on tropospheric ozone and radiative forcing: CTM calculations for the period 1990–2030, *Atmos. Chem. Phys.*, *5*, 1731–1755.

Dils, B., et al. (2005), Comparisons between SCIAMACHY and ground-based FTIR data for total columns of CO, CH_4, CO_2 and N_2O, *Atmos. Chem. Phys. Discuss.*, *5*, 2677–2717.

Dlugokencky, E., K. Masarie, P. Lang, and P. Tans (1998), Continuing decline in the growth rate of the atmospheric methane burden, *Nature*, *393*, 447–450.

Dlugokencky, E. J., B. P. Walter, K. A. Masarie, P. M. Lang, and E. S. Kasischke (2001), Measurements of anomalous methane increase during 1998, *Geophys. Res. Lett.*, *28*(3), 499–502.

Dlugokencky, E. J., S. Houweling, L. Bruhwiler, K. A. Masarie, P. M. Lang, J. B. Miller, and P. P. Tans (2003), Atmospheric methane levels off: Temporary pause or a new steady-state?, *Geophys. Res. Lett.*, *30*(19), 1992, doi:10.1029/2003GL018126.

Etheridge, D., L. Steele, R. Francey, and R. Langenfels (1998), Atmospheric methane between 1000 A.D. and present: Evidence of anthropogenic emissions and climate variability, *J. Geophys. Res.*, *103*(D13), 15,979–15,993.

Fletcher, M., S. Mikaloff, P. Tans, L. Bruhwiler, J. Miller, and M. Heimann (2004a), CH_4 sources estimated from atmospheric observations of CH_4 and its $^{13}C/^{12}C$ isotopic ratios: 2. Inverse modeling of CH_4 fluxes from geographical regions, *Global Biogeochem. Cycles*, *18*(4), GB4005, doi:10.1029/2004GB002224.

Fletcher, M., S. E. Mikaloff, P. Tans, L. Bruhwiler, J. B. Miller, and M. Heimann (2004b), CH_4 sources estimated from atmospheric observations of CH_4 and its $^{13}C/^{12}C$ isotopic ratios: 1. Inverse modeling of source processes, *Global Biogeochem. Cycles*, *18*(4), GB4004, doi:10.1029/2004GB002223.

Frankenberg, C., J. F. Meirink, M. van Weele, U. Platt, and T. Wagner (2005a), Assessing methane emissions from global space-borne observations, *Science*, *308*(5724), 1010–1014, doi:10.1126/science.1106644.

Frankenberg, C., U. Platt, and T. Wagner (2005b), Iterative maximum a posteriori (IMAP)-DOAS for retrieval of strongly absorbing trace gases: Model studies for CH_4 and CO_2 retrieval from near infrared spectra of SCIAMACHY on board ENVISAT, *Atmos. Chem. Phys.*, *5*, 9–22.

Frankenberg, C., U. Platt, and T. Wagner (2005c), Retrieval of CO from SCIAMACHY on board ENVISAT: Detection of strongly polluted areas and seasonal patterns in global CO abundances, *Atmos. Chem. Phys.*, *5*, 1639–1644.

Gedney, N., P. Cox, and C. Huntingtonford (2004), Climate feedback from wetland methane emissions, *Geophys. Res. Lett.*, *32*, L20503, doi:10.1029/2004GL020919.

Gloudemans, A., H. Schrijver, A. Straume, I. Aben, A. Maurellis, M. Buchwitz, R. de Beek, C. Frankenberg, and T. Wagner (2004), CH_4 and CO total columns from SCIAMACHY: Comparisons with TM3 and MOPITT, in *Proceedings ACVE2, 3–7 May, Frascati, Italy*, *ESA Spec. Publ., SP-562*.

Gloudemans, A. M. S., H. Schrijver, Q. Kleipool, M. M. P. van den Broek, A. G. Straume, G. Lichtenberg, R. M. van Hees, I. Aben, and J. F. Meirink (2005), The impact of SCIAMACHY near-infrared instrument calibration on CH_4 and CO total columns, *Atmos. Chem. Phys. Disc.*, *5*, 1733–1770.

Gonzalez, F., and H. Rodriguez (2000), Greenhouse-gas emissions in Colombia 1998–2010, technical report, Colombian Acad. of Sci., Santafé de Bogotá, Colombia.

Hansen, J., and M. Sato (2004), Greenhouse gas growth rates, *Proc. Natl. Acad. Sci. U. S. A.*, *101*(46), 16,109–16,114.

Hansen, J., M. Sato, R. Ruedy, A. Lacis, and V. Oinas (2000), Global warming in the twenty-first century: An alternative scenario, *Proc. Natl. Acad. Sci. U. S. A.*, *97*(18), 9875–9880.

Hao, W. M., M. H. Liu, and P. J. Crutzen (1991), Estimates of the annual and regional releases of CO_2 and other trace gases to the atmosphere from fires in the tropics based on the FAO statistics for the period 1975–1980, in *Fire in the Tropical Biota*, edited by J. Goldhammer, pp. 440–462, Springer, New York.

Heimann, M., and S. Körner (2003), The Global Atmospheric Tracer Model TM3, Model Description and Users Manual Release 3.8a, *Tech. Rep. 5*, Max Planck Inst. for Biogeochem. (MPIBGC), Jena, Germany.

Hein, R., P. J. Crutzen, and M. Heimann (1997), An inverse modeling approach to investigate the global atmospheric methane cycle, *Global Biogeochem. Cycles*, *11*(1), 43–76.

Houweling, S., F. J. Dentener, and J. Lelieveld (1998), The impact of nonmethane hydrocarbon compounds on tropospheric photochemistry, *J. Geophys. Res.*, *103*, 10,673–10,696.

Houweling, S., T. Kaminski, F. Dentener, J. Lelieveld, and M. Heimann (1999), Inverse modeling of methane sources and sinks using the adjoint of a global transport model, *J. Atmos. Res.*, *104*(D21), 26,137–26,160.

Houweling, S., W. Hartmann, I. Aben, H. Schrijver, J. Skidmore, G.-J. Roelofs, and F. M. Breon (2005), Evidence of systematic errors in SCIAMACHY-observed CO_2 due to aerosols, *Atmos. Chem. Phys. Discuss.*, *5*, 3313–3340.

Intergovernmental Panel on Climate Change (IPCC) (2000), Good practice guidance and uncertainty management in national greenhouse gas inventories, Kanagawa, Japan.

Intergovernmental Panel on Climate Change (IPCC) (2001), *Climate Change 2001: The Scientific Basis. Contribution of Working Group I to the Third Assessment Report of the Intergovernmental Panel on Climate Change*, 881 pp., Cambridge Univ. Press, New York.

Kneizys, F. X., et al. (1996), The MODTRAN 2/3 report and LOWTRAN 7 model, technical report, Phillips Lab., Geophys. Dir., Hanscom AFB, Mass.

Krol, M., S. Houweling, B. Bregman, M. van den Broek, A. Segers, P. van Velthoven, W. Peters, F. Dentener, and P. Bergamaschi (2005), The two-way nested global chemistry-transport zoom model TM5: Algorithm and applications, *Atmos. Chem. Phys.*, *5*, 417–432.

Lelieveld, J., P. J. Crutzen, and F. J. Dentener (1998), Changing concentration, lifetime and climate forcing of atmospheric methane, *Tellus, Ser. B*, *50*, 128–150.

Matthews, E., I. Fung, and J. Lerner (1991), Methane emission from rice cultivation: Geographic and seasonal distribution of cultivated areas and emissions, *Global Biogeochem. Cycles*, *5*, 3–24.

O'Brien, D. M., and P. J. Rayner (2002), Global observations of the carbon budget: 2. CO_2 column from differential absorption of reflected sunlight in the 1.61 μm band of CO_2, *J. Geophys. Res.*, *107*(D18), 4354, doi:10.1029/2001JD000617.

Olivier, J., and J. Berdowski (2001), Global emissions sources and sinks, in *The Climate System*, edited by J. Berdowski, R. Guicherit, and B. J. Heij, pp. 33–78, A. A. Balkema, Brookfield, Vt.

Olivier, J., J. Peters, C. Granier, G. Pétron, J. F. Müller, and S. Wallens (2003), Present and future surface emissions of atmospheric compounds, *POET Rep. 2, EU Proj. EVK2-1999-00011*.

Olivier, J. G. J., A. F. Bouwman, J. J. M. Berdowski, C. Veldt, J. P. J. Bloos, A. J. H. Visschedijk, C. W. M. Van der Maas, and P. Y. J. Zandveld (1999), Sectoral emission inventories of greenhouse gases on a per country basis as well as 1 × 1, *Environ. Sci. Policy*, *2*, 241–263.

Olsen, S. C., and J. T. Randerson (2004), Differences between surface and column atmospheric CO_2 and implications for carbon cycle research, *J. Geophys. Res.*, *109*, D02301, doi:10.1029/2003JD003968.

Pfeilsticker, K., F. Erle, O. Funk, H. Veitel, and U. Platt (1998), First geometrical pathlengths probability density function derivation of the skylight from spectroscopically highly resolving oxygen A-band observations: 1. Measurement technique, atmospheric observations, and model calculations, *J. Geophys. Res.*, *103*, 11,483–11,504.

Platt, U. (1994), Differential optical absorption spectroscopy (DOAS), in *Air Monitoring by Spectroscopic Techniques*, John Wiley, Hoboken, N. J.

Randel, W., F. Wu, J. Russell III, A. Roche, and J. Waters (1998), Seasonal cycles and QBO variations in stratospheric CH_4 and H_2O observed in UARS HALOE data, *J. Atmos. Sci.*, *55*, 163–185.

Rayner, P. J., R. M. Law, D. M. O'Brien, T. M. Butler, and A. C. Dilley (2002), Global observations of the carbon budget: 3. Initial assessment of the impact of satellite orbit, scan geometry, and cloud on measuring CO_2 from space, *J. Geophys. Res.*, *107*(D21), 4557, doi:10.1029/2001JD000618.

Ridgwell, A. J., S. J. Marshall, and K. Gregson (1999), Consumption of atmospheric methane by soils: A process-based model, *Global Biogeochem. Cycles*, *13*, 59–70.

Rodgers, C. (1976), Retrieval of atmospheric temperature and composition from remote measurements of thermal radiation, *Rev. Geophys.*, *14*, 609–624.

Rodgers, C. D. (2000), *Inverse Methods for Atmospheric Sounding*, World Sci., Hackensack, N. J.

Rothman, L., et al. (2005), The HITRAN 2004 molecular spectroscopic database, *J. Quant. Spectrosc. Radiat. Transfer*, *96*(2).

Sanderson, M. (1996), Biomass of termites and their emissions of methane and carbon dioxide: A global database, *Global Biogeochem. Cycles*, *10*, 543–557.

Shindell, D., B. Walter, and G. Faluvegi (2004), Impacts of climate change on methane emissions from wetlands, *Geophys. Res. Lett.*, *31*, L21202, doi:10.1029/2004GL021009.

Shindell, D. T., G. Faluvegi, N. Bell, and G. A. Schmidt (2005), An emissions-based view of climate forcing by methane and tropospheric ozone, *Geophys. Res. Lett.*, *32*, L04803, doi:10.1029/2004GL021900.

Takahashi, T., et al. (2002), Global sea-air CO_2 flux based on climatological surface ocean pCO_2, and seasonal biological and temperature effects, *Deep Sea Res.*, *49*, 1601–1622.

Van Aardenne, J. A., F. J. Dentener, C. G. M. Klein Goldewijk, J. Lelieveld, and J. G. J. Olivier (2001), A 1×1 degree resolution data set of historical anthropogenic trace gas emissions for the period 1890–1990, *Global Biogeochem. Cycles*, *15*, 909–928.

Wagner, T., S. Beirle, C. V. Friedeburg, J. Hollwedel, S. Kraus, M. Wenig, W. Wilms-Grabe, S. Kühl, and U. Platt (2002), Monitoring of trace gas emissions from space: Tropospheric abundances of BrO, NO_2, H_2CO, SO_2, H_2O, O_2, and O_4 as measured by GOME, in *Air Pollution 2002*, vol. 10, pp. 463–472, WIT Press, Southampton, U.K.

Wagner, T., J. Heland, M. Zöger, and U. Platt (2003), A fast H_2O total column density product from GOME - Validation with in-situ aircraft measurements, *Atmos. Chem. Phys.*, *3*, 651–663.

Walter, B., M. Heimann, and E. Matthews (2001), Modeling modern methane emissions from natural wetlands: 1. Model description and results, *J. Geophys. Res.*, *106*(D24), 34,189–34,206.

Worthy, D., I. Levin, F. Hopper, M. Ernst, and N. Trivett (2000), Evidence for a link between climate and northern wetland methane emissions, *J. Geophys. Res.*, *105*, 4031–4038.

Zimmermann, P., J. Greenberg, S. Wandiga, and P. Crutzen (1982), Termites: A potentially large source of atmospheric methane, carbon dioxide and molecular hydrogen, *Science*, *218*, 563–565.

P. Bergamaschi, European Commission Joint Research Centre, I-21020 Ispra, Italy.

C. Frankenberg, U. Platt, and T. Wagner, Institute of Environmental Physics, Department of Physics, University of Heidelberg, INF 229, D-69120 Heidelberg, Germany. (cfranken@iup.uni-heidelberg.de)

A. P. H. Goede, J. F. Meirink, and M. van Weele, Section of Atmospheric Composition, Royal Netherlands Meteorological Institute, NL-3730 De Bilt, Netherlands.

M. Heimann and S. Körner, Max Planck Institute for Biogeochemistry (MPI-BGC), D-07701 Jena, Germany.